Simplified model for absorber feature transmissions on EUV masks

Michael Lam, Andrew Neureuther

Michael C. Lam, Andrew R. Neureuther, "Simplified model for absorber feature transmissions on EUV masks," Proc. SPIE 6349, Photomask Technology 2006, 63492H (20 October 2006); doi: 10.1117/12.686209

SPIE.

Event: SPIE Photomask Technology, 2006, Monterey, California, United States

Simplified model for absorber feature transmissions on EUV masks

Michael C. Lam[1,2] and Andrew R. Neureuther[2]

[2]Department of Electrical Engineering and Computer Sciences
University of California- Berkeley, Berkeley, CA 94720

ABSTRACT

A new thin mask model for transmission through EUV absorber features is proposed, which, when linked to an EUV buried defect simulator, can rapidly assess a buried defect's impact on the printability of nearby features. The underlying physics of an absorber edge scattering is thoroughly investigated and simplified models for two of the key physical effects are shown to produce excellent results when compared to FDTD edge scattering. By simply adding calibrated line sources to the top corners of the absorber edges, as well as propagating the thin mask by about half the mask thickness, a greatly simplified model for feature transmissions is produced. The simplified model effectively converts the electrically thick nature of the absorber patterns (~70nm or ~5λ thick) into a thin mask model, while capturing all of the appropriate effects that are demonstrated in the far field image. Line and space example patterns for dense 32nm, 22nm, and 15nm features (on wafer) demonstrate the accuracy of the new thin mask model for even very tight pitches.

1. BACKGROUND

Various fast simulation methods have been proposed [1,2,3,4] for modeling EUV photomasks over traditional, slow electromagnetic field (EMF) techniques [5]. Some of these promising techniques only tackle half of the full EUV scattering problem by simulating only multilayer defects without absorber features present. A full simulation solution is highly desirable that would include the impact of absorber features with the buried defects. The complete EUV photomask scattering problem is shown schematically in Figure 1 and can be decomposed into two smaller problems: 1) a transmission through the absorber features and 2) a reflection from a non-planar multilayer. Evanschitzky [3] has also noted a similar decomposition can effectively handle the full scattering problem by linking FDTD transmission through absorber features to a simplified model for defective multilayers. The ray tracing methodology developed in [4] has already been demonstrated to effectively handle the second part of the EUV scattering problem, and so a fast and accurate method for handling the transmission through the absorber features is all that is needed to completely model the problem. The methodology in [4] will be referred to as the buried defect simulator in this paper.

Once appropriate methodologies have been identified for each part of the problem, they can be linked together by the flow chart in Figure 2. An incident plane wave onto the example structure in Figure 1 can be reflected and transmitted through the absorber features via an appropriate simulator. The electric fields below the absorber features can be Fourier transformed into its plane wave spectrum and each plane wave fed into the buried defect simulator[4]. The total reflection from the defective multilayer can again be Fourier transformed into its plane wave spectrum and each plane wave transmitted upward through the absorber features a second time. In this manner the electric fields have been doubly diffracted by the absorber features during the downward and upward pass [6]. The total scattering from the EUV problem can then be made by adding the initial reflection from the absorber features with the final output of the doubly diffracted electric fields. This simple process ignores any secondary coupling between the absorber features and the multilayer reflection. A full scattering matrix approach could also be used to understand multiple re-reflections between the absorber features and the multilayer structure. This approach would cause a significant increase in the computation time since each individual plane wave would

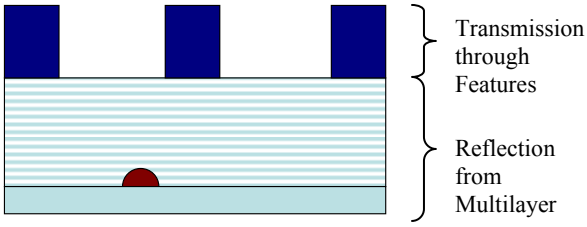

Figure 1. EUV photomask domain with absorber features placed on top of a multilayer reflection stack. A buried defect is shown sitting below the multilayers.

[1] Mentor Graphics, Michael_lam@mentor.com

Photomask Technology 2006, edited by Patrick M. Martin, Robert J. Naber,
Proc. of SPIE Vol. 6349, 63492H, (2006) · 0277-786X/06/$15 · doi: 10.1117/12.686209

couple into a set of many diffracted plane waves. However, the reflected fields computed from both objects for each angle of incidence could be reused for each additional reflection that occurs. It is anticipated that these second order effects are relatively small, since the reflection from the absorber features is on the order of 4% and should decay very quickly upon re-reflection. Of final note, the initial incident plane wave can be generalized to a set of plane waves to account for partial coherence incident on the mask. The above process would then be repeated for each plane wave.

The full process outlined in Figure 2 will undoubtedly take longer to fully simulate an EUV structure than the buried defect simulator alone. While the additional step of creating a thin mask transmission function will not add appreciably to the runtime, the buried defect simulator will have to be run multiple times to properly reflect the diffracted fields passing down through the absorber features. A single incident plane wave will transmit through the absorber and be diffracted into a new set of *n* plane waves which each must be simulated with the buried defect simulator. Each of the *n* plane waves incident on the multilayer will produce another *n* plane waves that must be propagated upwards through the absorber features. In this sense, the full method will need to run the buried defect simulator at least *n* times, and thus should be at least *n* times slower when simulating features on top of a buried defect. A good estimate for a large 3D simulation would be about 50-100 times slower.

All of the simulations performed in this paper assume that the absorber features are 70nm in height and made of TaN with a refractive index at $\lambda = 13.4$nm of $n_{TaN} = 0.9272128642 - j*0.0429253317$. The multilayer has 40 bilayers and each bilayer having a total thickness of 6.9nm, with a silicon thickness of $t_{si} = 4.14$nm and molybdenum thickness of $t_{mo} = 2.76$nm.

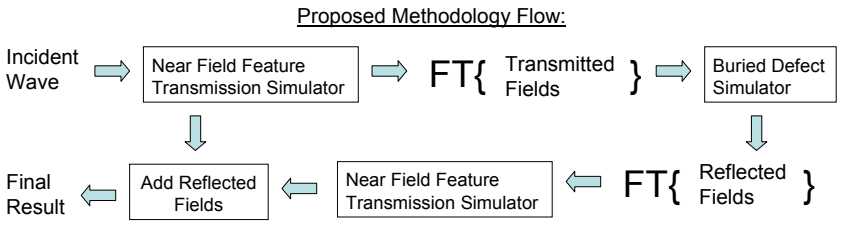

Figure 2. Proposed methodology flow for linking feature printability and buried defect printability.

2. ANALYSIS OF PHYSICAL EDGE SCATTERING

Before developing an appropriate model for transmission through the absorber features, the physical mechanisms that occur during transmission must be characterized and understood. There are three distinct regions in Figure 3 that must be analyzed to understand the transmission through the absorber features. First, a large dark area of absorber can be simply understood and characterized by understanding the transmission and reflection from a single bilayer made of the absorber material with the absorber's thickness. Second, a large open area of the photomask can easily be understood by simply propagating the incident plane wave in free space by a distance equal to the absorber thickness. The last region consists of the area in the vicinity of an absorber edge. This region is the most interesting electromagnetically and the most complicated to understand. FDTD analysis will aid in verifying some of the physical characteristics that can be expected from scattering near an edge.

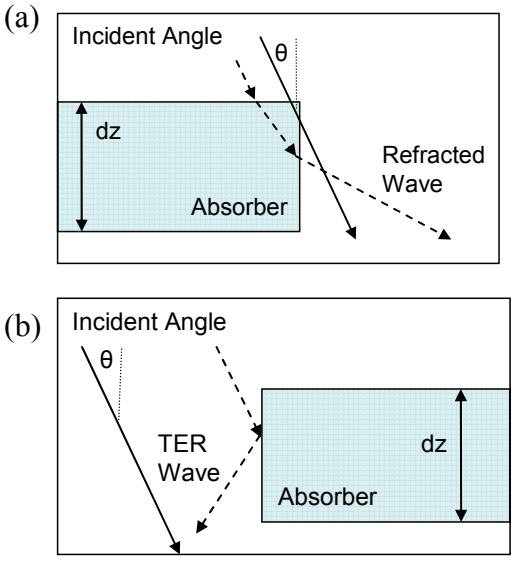

Figure 3. Definitions of (a) left absorber edge and (b) right absorber edge.

A simple manner to probe the edge scattering effects is to take the large dark area solution (a thick bilayer) and the large open area solution (propagating a wave in free space) and place each one next to an edge. This analysis forces two imposed solutions on Maxwell's equations on each side of the edge. Maxwell's equations will then respond to these imposed solutions, creating additional fields that will simply add via superposition to make the imposed solutions satisfy the appropriate boundary conditions at the edge interface. These additional fields can be viewed as physical response fields associated with approximating a thick mask scattering problem with a thin mask model based on vertical propagation. These response fields must also be modeled to fully calculate the near field transmission.

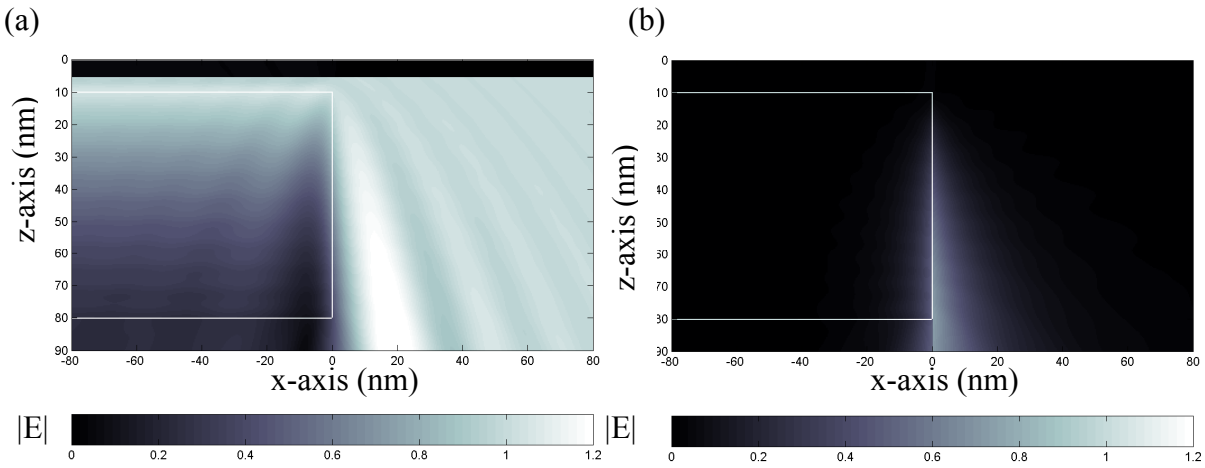

Figure 4. (a) |E| for isolated left absorber edge with absorber outline, (b) |E| of error field for isolated left absorber edge with absorber outline.

Two types of edges, a left edge and a right edge, will have to be investigated to deal with the edge orientation relative to off-axis illumination. A left edge is defined in this analysis as an edge with absorber on the left and air on the right with the incident light coming across the edge from left to right, as shown in Figure 3a. A right edge is defined in this analysis as an edge with absorber on the right and air on the left with the incident light coming across the edge from left to right, as shown in Figure 3b. Each type of edge can be analyzed under normal incidence and off-normal incidence.

Under normal incidence light, both a left edge and a right edge behave as mirror images of each other, so only a left edge will be investigated. The first half of the imposed solution, the light propagating down on the air side of the edge, will have to set up a new set of fields within the absorber to satisfy the boundary conditions on the edge. Snell's Law and the Fresnel Equations [7] show that the plane wave propagating down the interface will have a transmission coefficient of 0 along the interface, showing that no energy is transferred across the vertical interface and an evanescent wave is set up in the absorber that decays exponentially laterally into the absorber but propagates vertically down the edge interface. The second imposed solution, a plane wave propagating vertically down the interface in the absorber region, the plane wave will actually refract out of the absorber material and begin propagating in the air at an angle of about 23º relative to the vertical. This angle can be directly calculated by solving [7] for θ_2 given $\theta_1 = 90º$. These two effects can be seen in Figure 4, where FDTD has simulated a TE plane wave scattering from an isolated left absorber edge. Figure 4a shows the total electric fields in the vicinity of the edge, while Figure 4b shows the total electric fields of

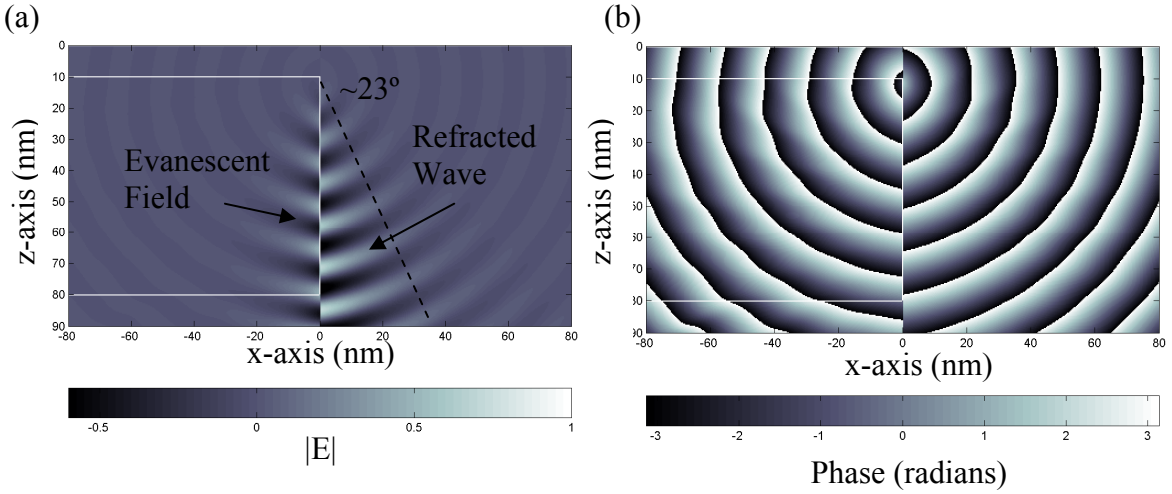

Figure 5. (a) Instantaneous error field for isolated left absorber edge with absorber outline at normal incidence, (b) Phase of error field for isolated left absorber edge with absorber outline at normal incidence.

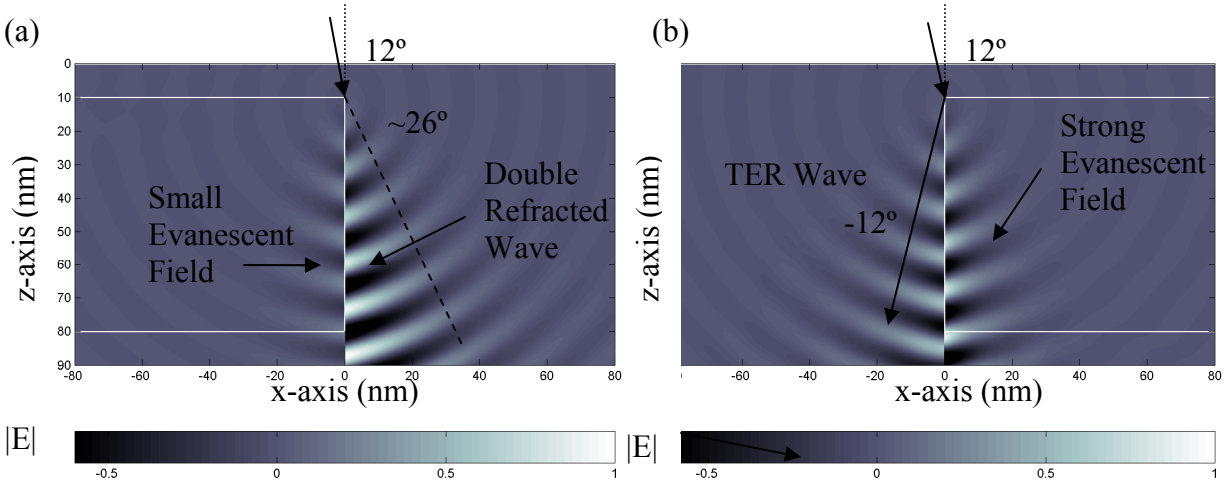

Figure 6. (a) Instantaneous error field for isolated left absorber edge with absorber outline for a 12º incident wave, (b) Instantaneous error field for isolated right absorber edge with absorber outline for a 12º incident wave.

an edge with the imposed solutions subtracted out. Obviously from Figure 4b, the response fields from imposing these two solutions come from the edge effects, which were expected.

The physical response fields can be further analyzed by looking at their phase and instantaneous magnitudes. On the left of the edge location in Figure 5, an evanescent field is set up inside of the absorber while a refracted transmitted wave is being generated on the right side of the edge location in air. These effects are the two, first-order corrections to the imposed solutions described above. The refracted wave's angle can be measured and it appears to be traveling at approximately 23º which was predicted. Another interesting effect is seen in Figure 5a whereby a point source is actually radiating from the top corner of the absorber edge. Figure 5b confirms the cylindrical nature of the point source by looking at the phase of the error fields.

A left and right edge can be analyzed at an off-axis angle by looking at FDTD simulations as well. A left edge will still have a refracted wave propagating from the absorber material into the air region due to the double refraction at the top surface and the edge interface. The angle of the refracted wave will be larger with an off-axis incident wave since the additional incident angle will provide an even larger refracted angle. The evanescent field within the absorber material, however, will be greatly diminished with angle due to the shadow region created by the thick absorber feature. Figure 6a shows the response fields for a left absorber edge for an incident off-axis plane wave. The double refracted wave is clearly seen and the evanescent field inside the absorber is significantly reduced. A point source at the top corner of the absorber is also present, just like at normal incidence. A right edge will have some interesting changes at off-normal incidence. First, the incident light impinging on the edge will be totally externally reflected (TER) from the edge interface for any incident angle less than 23º (note that this angle is consistent with the previous angle of minimum angular deviation for a refracted wave due to reciprocity). This reflection creates a wave propagating at the negative incident angle that folds back on top of the original incident wave. The TER at the interface also creates an evanescent field inside the absorber material. The refraction at the top surface of the absorber creates a shadow region in the absorber material that limits any refraction of light back out of the absorber into the air. Figure 6b shows the instantaneous response electric fields from a right absorber edge. The TER can be immediately seen to the left of the edge location and its angular spread is significantly less than the double refracted wave (which is absent from the right edge) for the left edge case. The evanescent field from the TER can also be seen inside of the absorber. A point source can once again be seen emanating from the top corner of the absorber edge.

3. SIMPLIFIED MODEL OF FEATURE TRANSMISSION

The simple thin mask transmission model that was used as an imposed solution on Maxwell's equations is the starting point of a simplified model for predicting the transmission of a plane wave through the absorber features. The physical response fields discussed in the above section represent the sources of error that the thin mask model makes relative to a rigorous solution for the diffraction scattering. It appears that significant errors are encountered when imposing the thin mask model onto the scattering from an isolated edge. Point sources, refracted fields, TER fields, and

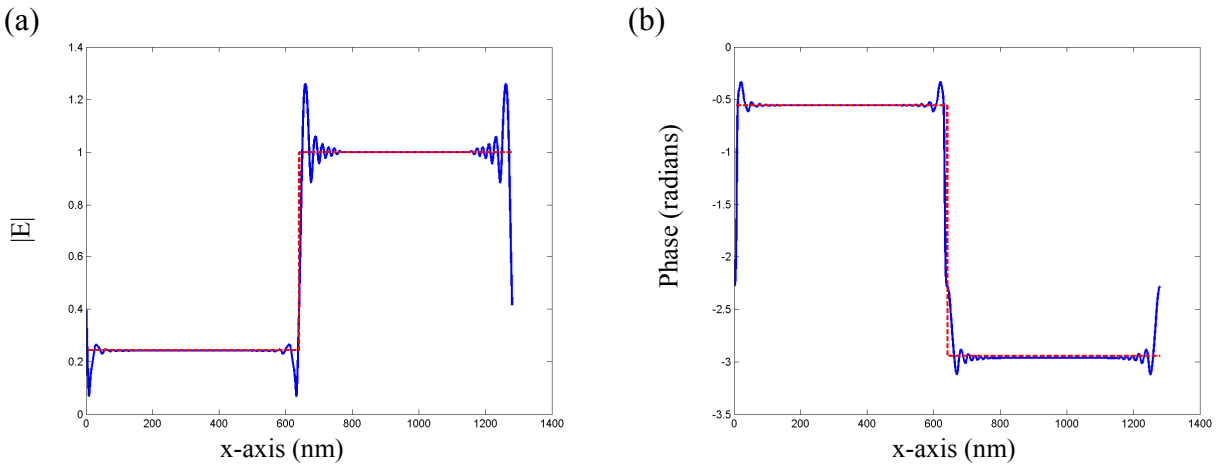

Figure 7. Cut lines below the absorber for the electric field from a normally incident plane wave. Solid blue lines are FDTD and red dashed lines are the thin mask model. (a) magnitude and (b) phase.

evanescent fields are all missing from the thin mask model and cause significant deviations to be encountered in the vicinity of an absorber edge. Each one of these effects would need to be accurately modeled and added to the thin mask approximation to obtain an accurate near field description of the edge scattering.

However, all except for one of these sources of error can be largely ignored in the far field image since their effects are mostly contained in the high spatial frequencies that scatter outside of the imaging optic. This limited angular collection will allow three of the four response fields to be neglected in a new scattering model. First, the evanescent fields are likely negligible in the far field due to the nature of evanescent fields and the high spatial frequency content of their laterally localized fields. Second, the refracted waves can also be largely ignored because they propagate at a minimum angle of 23º, which is significantly larger than the maximum collection angle of the EUV optic with an NA = 0.4. Similarly, the TER fields can be neglected because they propagate at negative the incident angle. This is because EUV systems are telecentric about 6º and the TER fields would scatter to an angle equal to their propagation angle plus 6º out of the center of the pupil. This argument means the TER fields will likely scatter outside of the pupil as well for incident angles greater than 3º. A sine effect can be used to argue that TER fields under 3º are also negligible since the amount of absorber edge that the incident fields actually see is proportional to the sine of the incident angle. Thus, the magnitude of those TER fields that are under 3º is likely very small. The point sources observed in Figures 5 and 6 cannot be neglected, however, since they fill the entire pupil of the imaging system and will definitely contribute some energy to the final observed image.

To prove that the above approximations are reasonable, cut lines of the thin mask model and the rigorous FDTD results must be compared. Figure 7 shows the calculated magnitude and phase of the near field transmissions of a normally incident plane wave for FDTD and the thin mask model for two edges separated by a large distance. The thin mask model is quite accurate far away from the edge locations, while significant errors are observed close to the edge. A better understanding of the errors can be obtained by looking at the spectrums of the two methods, as shown in Figure 8. For angles within a ±20º cone, the thin mask model is predicting very nice results compared with FDTD for all of the odd orders, but all of the even orders are wrong. The thin mask model assumes a perfectly odd function describes the transmission function, leaving all the even orders set to zero. From Fourier analysis, the even orders come from an even symmetry in the transmission function that is

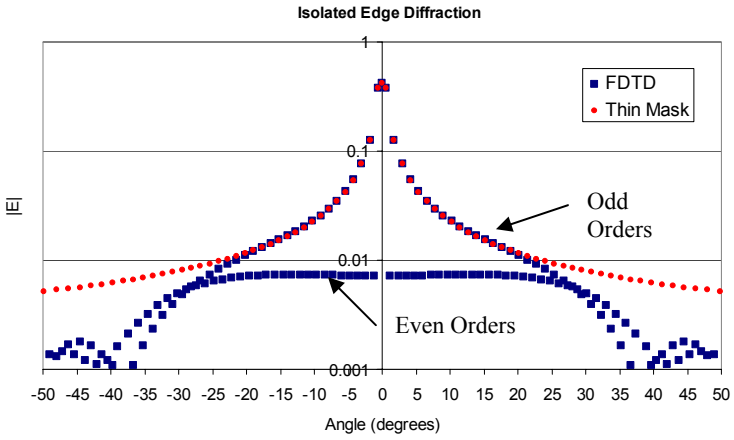

Figure 8. Angular spectrum of cut lines for two absorber edges very far apart for both FDTD and the thin mask model.

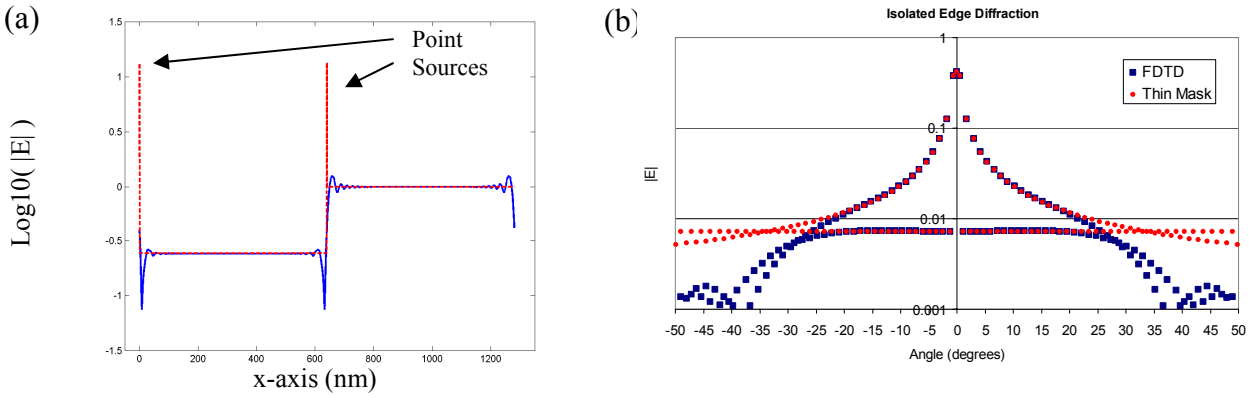

Figure 9. (a) New transmission function with corner point sources plotted on a $\log_{10}$ scale with the FDTD results. Solid blue lines are FDTD while red dashed are the thin mask model. (b) the spectrum of the two methods showing excellent agreement in all of the orders.

double the period of the original odd function. Figure 8 shows that the even orders are nearly flat across all the angles of interest, and so a simple model for these even orders is to simply add a constant background to the even orders that exactly matches those taken from the FDTD solution. Doing this and inverse Fourier transforming the constant even orders, results in a spatial representation of the error fields between FDTD and the thin mask model when looking inside a small angular cone. These error fields turn out to simply be shifted and scaled impulse functions that occur at the absorber edges! So in fact, the point sources observed in Figures 5 and 6 at the corners of the absorber are the only edge effects needed to improve the thin mask model. And these can be modeled by simply adding the scaled impulse functions to every edge in the simulation. Figure 9a shows a new transmission function with the corner point sources added plotted on a $\log_{10}$ scale, while Figure 9b shows the |E| of the spectrum from both FDTD and the improved thin mask model. The point sources can be more clearly seen on the log scale and provide a constant background in the even orders in the corresponding spectrum. In this manner, the corner point sources will need to be characterized for the type of material and thickness that is used for the absorber using a single FDTD simulation, but these point sources will then scale any arbitrary configuration. The point sources for the TaN absorber with thickness of 70nms are:

Equations 1, 2:

$$E_{TE\_pt\_source} = 13.35e^{-j0.140971}$$

$$E_{TM\_pt\_source} = 13.35e^{-j0.035537}$$

An investigation into the phase of the spectrum is needed to fully characterize an isolated edge scattering. Figure 10a shows the phases of the angular spectrums for the FDTD results and the improved thin mask model for a normally incident plane wave. Clearly the phases of the thin mask spectrum are significantly different from the phases of the FDTD results. The thin mask model has zero phase dependence on the angular spectrum while the FDTD has an almost parabolic dependence on spectrum angle. This effect most likely comes from the instantaneous aperturing assumptions built into a thin mask model. As its name suggests, a thin mask is infinitely thin and its effects on an incident plane wave are instantaneous. However, the EUV absorber features are very thick (~5λ) and take some propagation distance to actually arrive at their final values below the mask absorber. If the improved thin mask model is propagated forward by some distance z_o, the flat phase dependence will begin to take on the characteristic parabolic (or spherical wave) phase dependence for the angular spectrum. The propagation distance z_o will also depend on the material properties and thickness of the absorber, just like the corner point sources. However, the propagation distance can be characterized for the type of absorber and then used for arbitrary configurations of absorber edges. For the 70nm thick TaN absorber in these simulations, z_o = 40nm was found to match the spectrum phases very nicely, as seen in Figure 10b. The 40nms seems reasonably valid since it represents about half the absorber thickness.

The simple model proposed above should work for off-axis illumination as well, since the point sources are relatively independent of angle of incidence. The constant spectrum approximation can therefore be used as a simple way to model off-axis illumination. The final methodology for obtaining a thin mask model of transmission through EUV absorber features is a four step process:

1) Create an on-axis, binary transmission function by looking at the transmission through a large open area and a large dark area of the mask.

2) Add scaled impulse functions to every edge in the pattern.
3) Shift the 0^{th} order of the transmission function to the appropriate incident angle.
4) Propagate the orders by z_o and inverse Fourier transform to obtain the near fields.

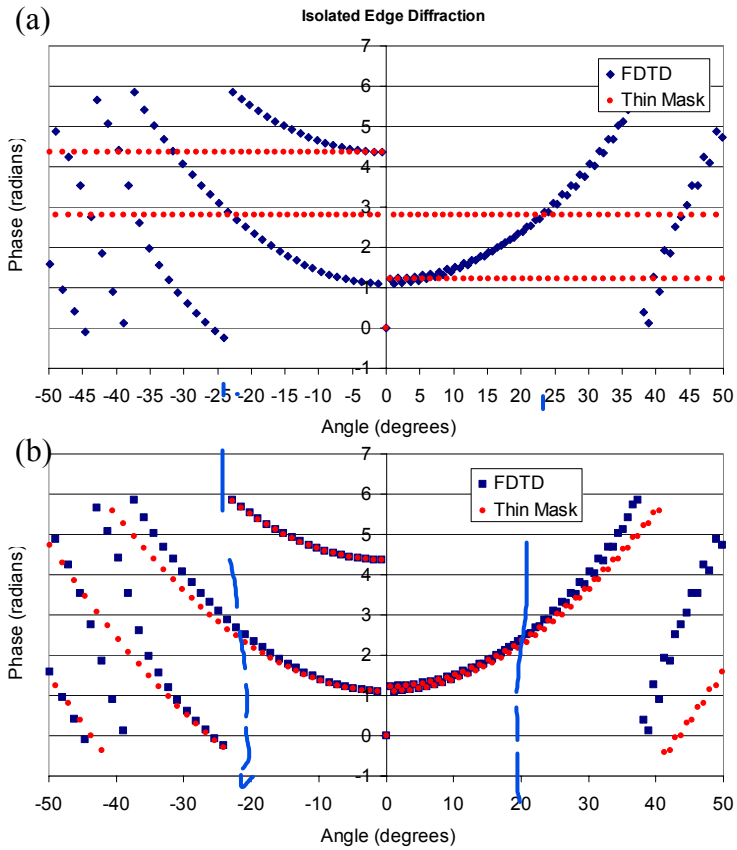

Figure 10. (a) Spectrum phases of thin mask model and FDTD without propagation (b) Spectrum of phases of thin mask model and FDTD with 40nm propagation.

4. EXAMPLES: DENSE LINE AND SPACE PATTERN TRANSMISSIONS

The simplified model for a thin mask transmission function described in the previous Section worked very well for modeling an isolated EUV absorber edge. It is only natural to question whether such a simple model will hold as feature edges become significantly closer together. This Section provides several examples of feature transmissions through dense line and space patterns. Since the targeted entry of EUV lithography is below the 32nm node, three line space patterns (32nm, 22nm, and 15nm features on wafer) will be tested for both polarizations at three different angles of incidence (0º, ~6º, ~12º), resulting in 18 test cases.

The 32nm line and space pattern actually has dimensions of 128nm on the mask (4X magnification). To properly compare the FDTD and thin mask model results, the final transmissions can be filtered down to only those plane waves physically entering a NA=1.0 system operating at 4X reduction, resulting in an angular collection cone of about ±15º. Since real EUV systems will operate at significantly reduced NA's, the true results are expected to be even better than those compared here. Figure 11 shows the filtered near field magnitude and phase for the TE polarization at various angles of incidence on the mask. Clearly, the thin mask model does an exceptional job of modeling the FDTD results for 0º and 6º, however, the model becomes less accurate as the angles approach the more oblique 12º angles. While the TM data is not shown, the thin mask model works very well for this polarization as well.

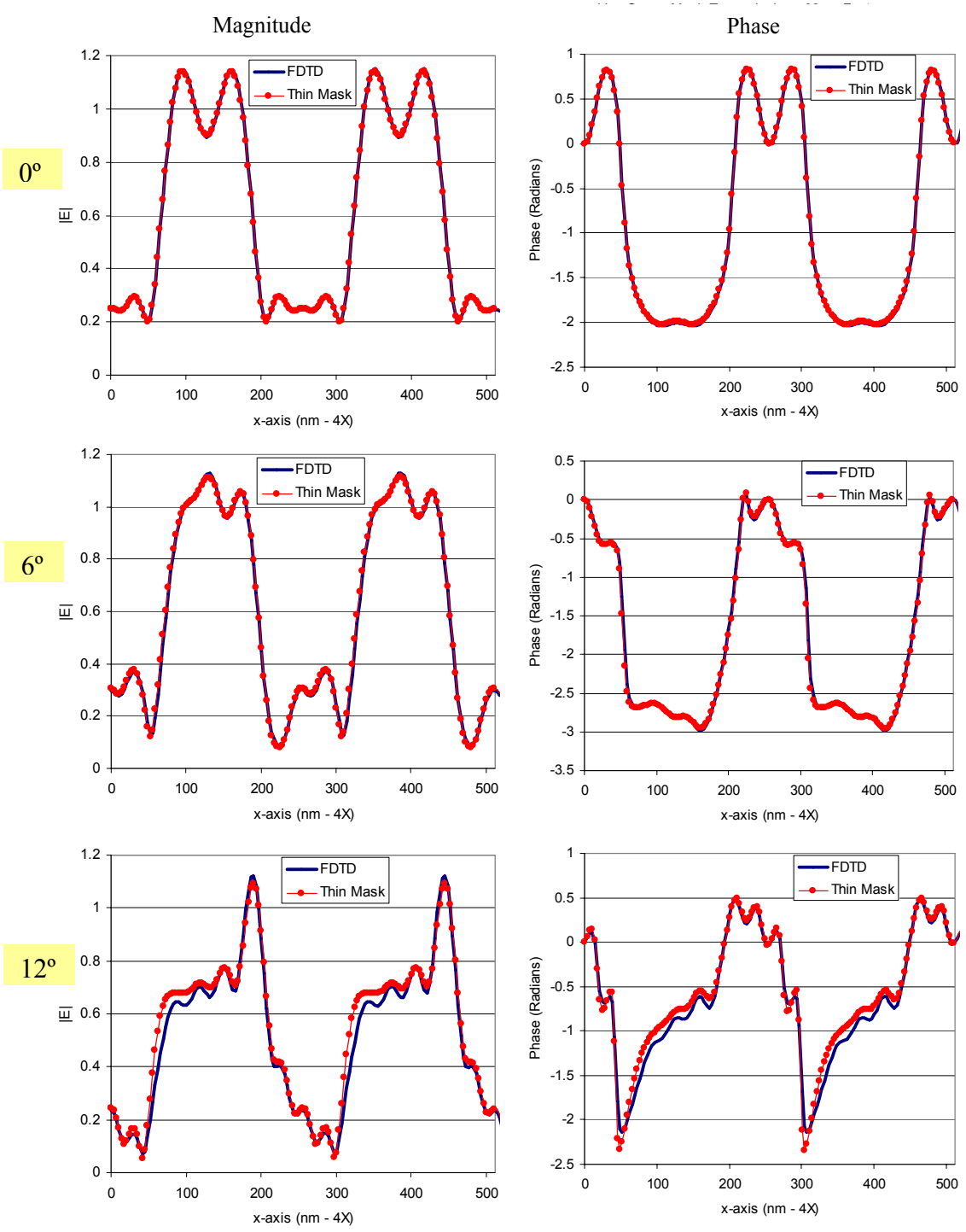

Figure 11. Filtered (NA = 1.0), coherent, near field transmissions of a TE plane wave for various angles of incidence through line space patterns giving 32nm features on the wafer.

Near Fields. TE Polarization. 22nm Features

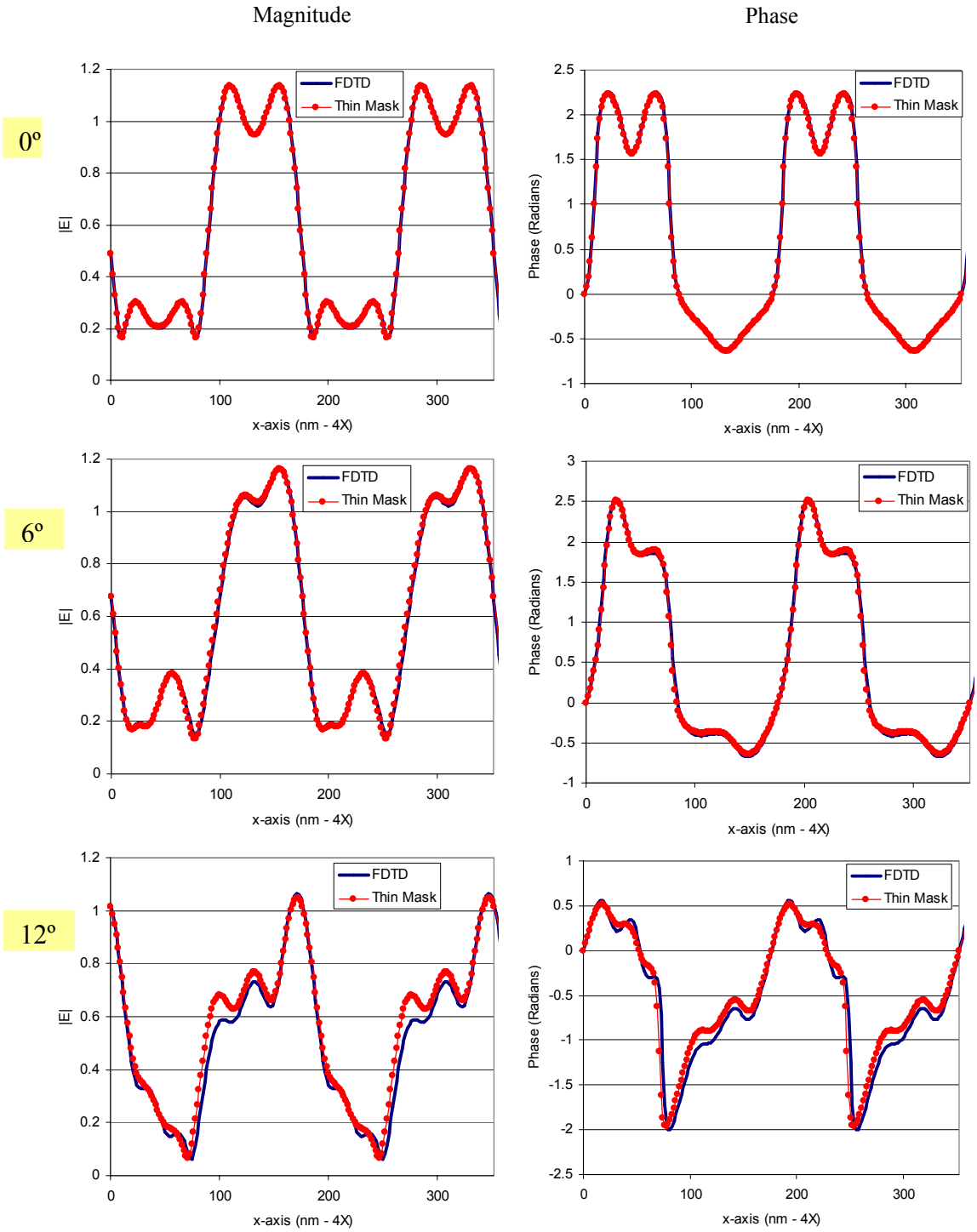

Figure 12. Filtered (NA = 1.0), coherent, near field transmissions of a TE plane wave for various angles of incidence through line space patterns giving 22nm features on the wafer.

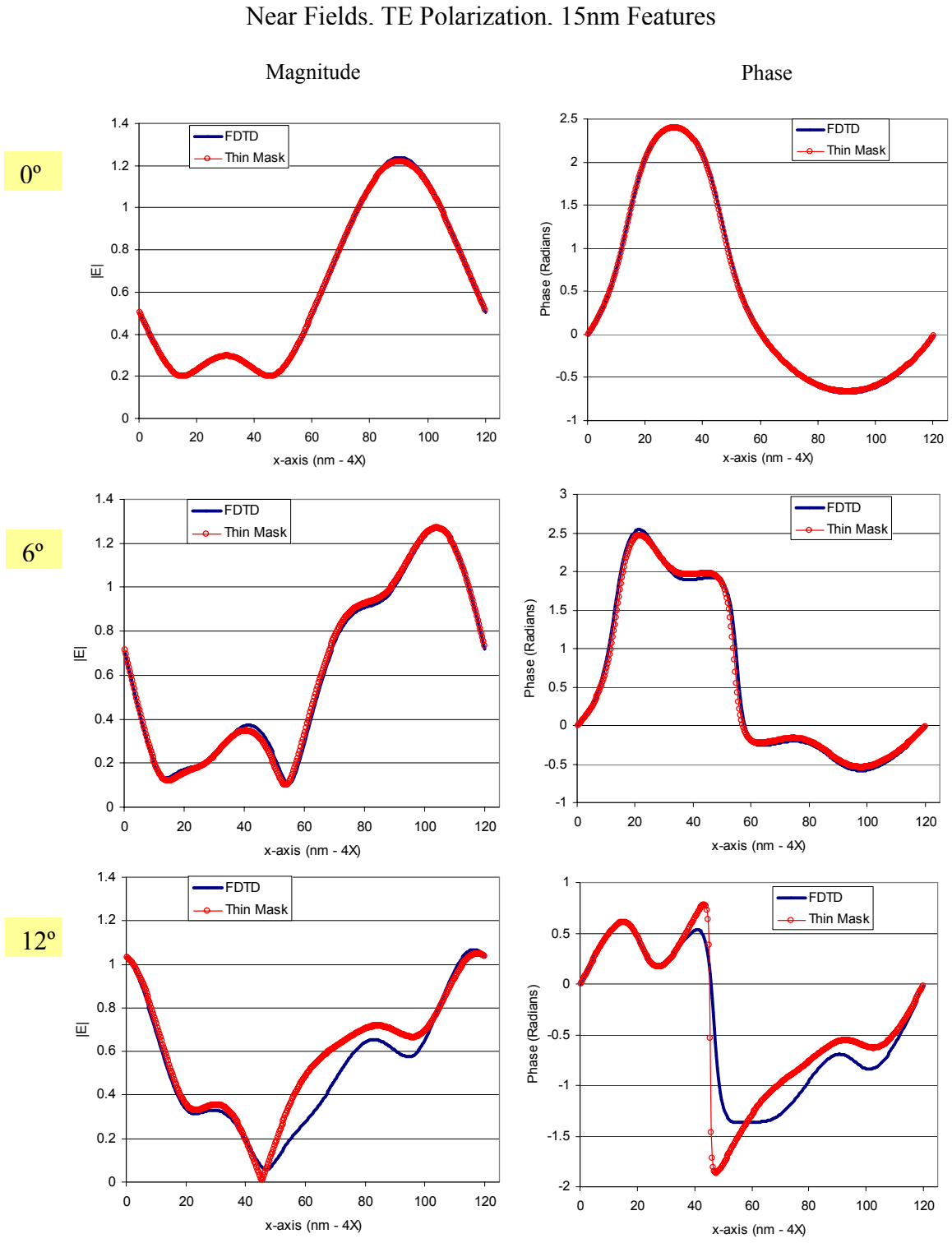

Figure 13. Filtered (NA = 1.0), coherent, near field transmissions of a TE plane wave for various angles of incidence through line space patterns giving 15nm features on the wafer.

The 22nm line and space pattern actually has dimensions of 88nm on the mask (4X magnification). Again, the near fields can be filtered down to an angular collection cone of about ±15º. Figure 12 shows the filtered near fields for the TE polarization for various angles of incidence on the mask. Once again, the thin mask model does an exceptional job of modeling the 0º and 6º angles, while the model becomes less accurate as the angles approach more oblique incidence. While the TM data is not shown, the thin mask model works very well for this polarization as well.

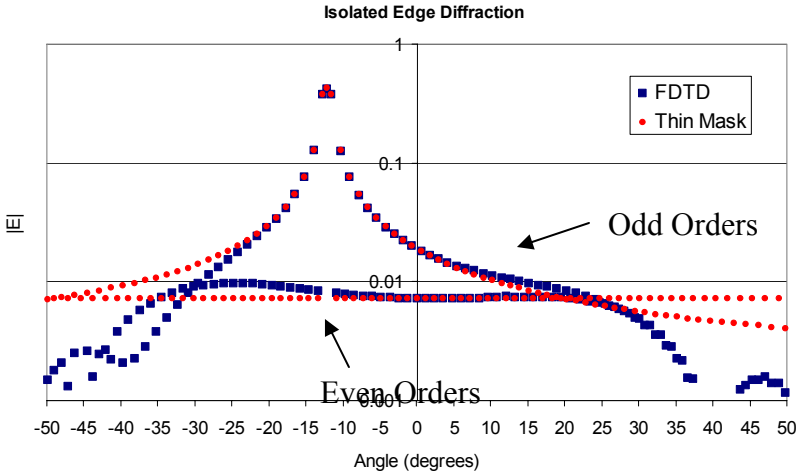

Figure 14. Angular spectrum of cut lines for two absorber edges very far apart for both FDTD and the thin mask model.

Finally, a very aggressive 15nm line and space pattern was tested which actually has dimensions of 60nm on the mask (4X magnification). Figure 13 shows the filtered (±15º) near fields for the TE polarization at various angles of incidence on the mask. Even at these very small feature sizes, the thin mask model predicts the filtered near fields very well for the 0º and 6º fields, while the 12º fields become significantly prone to errors. While the TM data is not shown, the thin mask model works very well for this polarization as well.

The above examples show that a simplified model for absorber feature transmission can be implemented and have extremely good accuracy. All the structures tested began to lose accuracy as the angles approached more oblique 12º. Most likely the simple point source model begins to break down at higher angles of incidence, and a more complicated model that takes into account the angular dependency of the point source will have to be implemented if higher accuracy is desired. To confirm this, an isolated edge illuminated at 12º incidence can be use to observe what happens to the even orders. Figure 14 shows the magnitude of the diffracted spectrum from the isolated edge with a 12º incident plane wave. The even orders begin to become asymmetrical for off-axis illumination and this is a likely cause for the errors observed in the above examples. The examples also show absorber edges on EUV masks can be modeled as independent edges with very little interactions on a single transmission through the features. Dense line and space features down to 15nm were shown to be sufficiently independent to allow the thin mask model to accurately approximate the transmission.

As a final proof of concept, the total reflection from a defect free 32nm line and space pattern will be calculated according to the procedure outlined in Figure 2 and compared to a full FDTD simulation for the same pattern. Figure 15

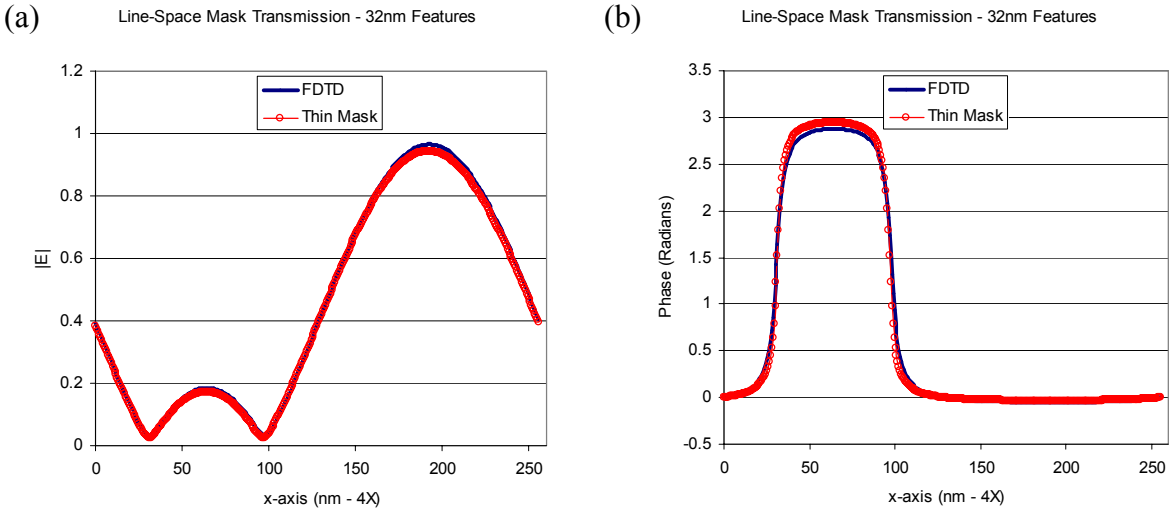

Figure 15. Full reflection from a 32nm line and space pattern for FDTD and the thin mask model linked to analytic calculations of reflection from a perfect multilayer structure. (a) Magnitude, (b) Phase.

shows the final reflected electric fields which have been filtered down to only those waves entering a 4X system centered at 0º with an NA = 0.4. Clearly, the thin mask model and FDTD are agreeing very well, and so this method for simulating features has been verified.

6. CONCLUSIONS

A complete methodology was proposed for simulating the impact of buried defects on absorber feature printability. The methodology relied on breaking the full EUV scattering problem into two simpler parts: 1) a transmission through the absorber features, and 2) the reflection from a non-planar multilayer. A simplified thin mask transmission model was introduced to solve the first part of the scattering problem, which could then be coupled to a buried defect simulator to solve the full EUV scattering problem. The thin mask model was derived from investigations of the physical edge scattering associated with a thick (~5λ) mask. Studies of the additional physical contributions from edges showed to first order, that only one out of the four observed physical effects contribute non-negligible energy to the final transmitted fields. The response fields could therefore be accurately approximated in the thin mask model by only including point sources that scatter from the top corners of the absorber material. The thin mask model must also be propagated vertically to account for the mask thickness. The magnitude and phase of the modeled point sources can be characterized based on the type and thickness of material used for the absorber. Additionally, the vertical propagation distance must be characterized based on the same parameters, but is expected to be about half the mask thickness.

The thin mask model was tested on the transmissions through 32nm, 22nm, and 15nm (wafer dimensions) line and space patterns to confirm its accuracy. The thin mask model works very well for all of the line and space patterns, demonstrating that it should be sufficient to model absorber features for a few generations. However, the accuracy of the model does depend fairly strongly on the angle of incidence on the mask. For angles approaching about 12º incidence, the thin mask model begins to predict some erroneous results, but still gives a generally good idea of the behavior that can be expected. The breakdown of the method is likely do to the simple model used for the point sources at the corners of the mask. Asymmetries in the scattering of the point sources begin to occur at larger angles of incidence, and these effects will need to be modeled to achieve more accuracy at these oblique angles.

This paper only offered a proof of concept that feature transmissions could be linked into the multilayer reflection. Much work is still needed to be done to characterize the material and thickness effects of the mask absorber on the generation of the thin mask model. More detailed studies will also need to be performed to investigate the accuracy of linking the features to the multilayer reflection. Investigations into the numerical dispersion of FDTD and its effect on propagation through a thick absorber feature and the reflection from the multilayer will need to be accomplished to better understand sources of error when comparing the linked fields with FDTD simulations.

ACKNOWLEDGEMENT

This research was supported by a grant from Intel.

REFERENCES

1. Ito, M., et al., “Simulation of multilayer defects in extreme ultraviolet masks.” Japanese Journal of Applied Physics Part 1, 2001. 40(4A): p. 2549-53.
2. Besacier, M., et al. “The Rayleigh method applied to EUV lithography simulation.” Proc. of SPIE, vol. 5037, 2003.
3. Evanschitzky, P., et al. “Simulation of extreme ultraviolet masks with defective multilayers.” Proceedings of Spie, vol.5130, no.1, 26 Aug. 2003, pp.1035-45.
4. Lam, MC and AR Neureuther, “A 3D substrate and buried defect simulator for EUV mask blanks.” SPIE, vol. 5751, 2005.
5. A. Wong, “Rigorous Three-Dimensional Time-Domain Finite-Difference Electromagnetic Simulation,” Ph.D. Dissertation, University of California at Berkeley, 1994.
6. Bollepalli, B.S. and F. Cerrina. “On the computation of reflected images from extreme ultraviolet masks.” Proceedings of Spie, vol.3676, 1999, pp.587-97.
7. M. Born and E. Wolf, *Principles of Optics, 7th (Expanded) Edition*, (Cambridge University Press, 1999), p. 40. Equation 8, 20, 21.